BOUNDARY LAYER EFFECTS ON THE CRITICAL NOZZLE OF HYDROGEN SONIC JET

Afroosheh, M.[1], Vakilimoghadda, F.[2] and Paraschivoiu, M.[3]

[1] Department of Mechanical and Industrial Engineering, Concordia University, 1455 De Maisonneuve Blvd W., Montreal, H3G 1M8, Canada, m_afroos@encs.concordia.ca
[2] Department of Mechanical and Industrial Engineering, Concordia University, 1455 De Maisonneuve Blvd W., Montreal, H3G 1M8, Canada, vakili.farbod@gmail.com
[3] Department of Mechanical and Industrial Engineering, Concordia University, 1455 De Maisonneuve Blvd W., Montreal, H3G 1M8, Canada, marius.paraschivoiu@concordia.ca

ABSTRACT

When hydrogen flows through a small finite length constant exit area nozzle the viscous effects create a fluid throat which acts as a converging-diverging nozzle and lead to Mach number greater than one at the exit if the jet is under-expanded. This phenomenon influences the mass flow rate and the dispersion cloud size. In this study, the effect of the pipe boundary layer on the unsteady hydrogen sonic jet from a high pressure reservoir (up to 70 MPa) is studied using computational fluid dynamics with a large eddy simulation turbulence model. This viscous flow simulation is compared with a non-viscous simulation to demonstrate that the velocity is supersonic at the exit of a small exit nozzle and that the mass flow is reduced.

1.0 INTRODUCTION

Compressed hydrogen is a common approach to store hydrogen, therefore many researchers study the behaviour of hydrogen upon release from a pressurized reservoir [1,2,3,4]. The common approach is to simulate this flow as a sonic flow through the nozzle. This assumption is quite reasonable as the flow can be approximated as an inviscid flow at the exit of the nozzle nevertheless we will show in this paper that this approach underestimates the exit flow velocity. Furthermore, the notional nozzle approach is often used to reduce the computational cost of simulating the flow downstream of the jet [5]. The notional nozzle approaches model the sonic jet to avoid the large computational cost of simulating the jet, therefore it is important to use a correct prediction of this jet.

For under-expanded jet flows, the viscous boundary layer in the nozzle creates a fluid throat. At the entrance of the exit straight pipe, the boundary layer thickness starts to grow. When reaching the exit, the boundary layer thickness decreases. This phenomenon creates a converging – diverging nozzle that drives the flow to Mach number greater than one [6,7]. The straight pipe acts as a critical nozzle. The discharge coefficient of a hydrogen gas flows through critical nozzles can be measured and predicted accurately with both analytical [8] or computational approaches [9] nevertheless the study of an effective critical nozzle existing in a straight pipe is new. It is known that the wall boundary layer effects have significant influence on lower Reynolds flow. Von Lavante [10] reported that nozzles of smaller than 1 mm in diameter suffer from higher measurement uncertainties when Reynolds number would be less than 3000.

Computational Fluid Dynamics has become an important tool to study the under-expanded jet. Significant work has been performed to numerically study the near-field of under-expanded gas jets and comparison with experimental data show good validity of this tool [11]. For high pressure reservoirs, Mohamed et al. [1] and Khaksarfard et al. [2] showed that for pressures higher than 10 MPa the real gas model is mandatory. Kim et al. [12] also reported with numerical simulations the effect of real gas behaviour of high pressure hydrogen gas (up to 50 MPa) on discharge coefficient of sonic nozzle. They concluded that by considering a real gas model, there will be a reduction on the discharge coefficient at high Reynolds numbers. Similarly, Nagao et al. [9] employed CFD to investigate the discharge coefficient of several real gases for high Reynolds flow. In addition, Morioka et al. [13] experimentally measured the discharge coefficient of hydrogen gas from a standard nozzle with pressure up to 70 MPa. More recent work has focused on numerically investigating this flow for

exit nozzles that are not cylindrical [14] as well as for high pressure reservoirs at low temperatures [15].
The present study aims at investigating the effects of viscous boundary layer inside the sonic release area, especially the effect on the flow Mach number and mass flow rate, considering high pressure hydrogen (up to 70 MPa) release into the atmosphere. The results will have great significance for further studies of viscous hydrogen release.

2.0 GOVERNING EQUATIONS AND NUMERICAL MODEL

For flow simulation of a compressible medium, the equation governing conservation of mass, momentum and energy must be solved. These equations should be filtered for turbulence modelling. Filtering an arbitrary function like *f* is defined as a convolution integral:

$$\bar{f}(\vec{x},t) = \iiint G\,(\vec{x}-\xi,\Delta) f\left(\vec{\xi},t\right) d^3\xi, \tag{1}$$

where Δ is the filter width, associated with mesh size as $\Delta = (\Delta x \Delta y \Delta z)^{1/3}$. In addition to velocity and pressure fluctuations, density and temperature fluctuations must be taken into account for compressible flow. Hence, instead of time averaging, Favre averaging operation is employed:

$$\tilde{f}(\vec{x},t) = \frac{\overline{\rho f}}{\bar{\rho}} \tag{2}$$

This filtering decomposes the various flow properties in terms of convectional mean and fluctuating part. Applying this averaging operation, the Favre averaged mean conservation equations are derived as in [3], [16] and [17]:

$$\frac{\partial \bar{\rho}}{\partial t} + \vec{\nabla}.\left(\bar{\rho}\vec{\tilde{v}}\right) = 0 \tag{3}$$

$$\frac{\partial \bar{\rho}\vec{\tilde{v}}}{\partial t} + \vec{\nabla}.\left(\bar{\rho}\vec{\tilde{v}}\vec{\tilde{v}}\right) = -\vec{\nabla}\bar{P} + \vec{\nabla}.(\vec{\tau} + \vec{\tilde{\sigma}}) \tag{4}$$

$$\frac{\partial \bar{\rho}\tilde{e}}{\partial t} + \vec{\nabla}.\left((\bar{\rho}\tilde{e} + \bar{P})\vec{\tilde{v}}\right) = \vec{\nabla}.\left(\vec{Q} + \frac{\mu\, C_p}{\mathrm{Pr}}\vec{\nabla}\bar{T} - \bar{\rho}\sum_j \bar{h}_j \overrightarrow{J_j} + \left(\vec{\tau} + \vec{\tilde{\sigma}}\right).\vec{\tilde{v}}\right) \tag{5}$$

Using this notation $\tilde{e}$ represents filtered total specific energy which is the summation of internal energy and kinetic energy.

$$\tilde{e} = \tilde{\imath} + \frac{1}{2}\left(\vec{\tilde{v}}.\vec{\tilde{v}}\right) \tag{6}$$

Also, $\bar{h}$ represents filtered total enthalpy of each species:

$$\bar{h} = \tilde{e} + \frac{\bar{P}}{\bar{\rho}} \tag{7}$$

An equation of state must be specified to close this set of equations. The Abel-Noble equation of state for real gas modelling is employed:

$$\bar{P} = \frac{\bar{\rho}R\bar{T}}{1 - b\bar{\rho}} \quad , \quad b = 0.00775\ {}^{m^3}/_{Kg} \tag{8}$$

$$\begin{Bmatrix} & R[\frac{J}{Kg\ K}] \\ Air & 287.097 \\ H_2 & 4124.18 \end{Bmatrix}$$

Assuming a Newtonian fluid, tensor of molecular viscous forces in (5) can be represented by the Boussinesq relation

$$\vec{\tilde{\sigma}} = \mu\left[\left(\vec{\nabla}.\vec{\tilde{v}} + \vec{\nabla}.\vec{\tilde{v}}^{T}\right) - \frac{2}{3}\vec{\nabla}.\vec{\tilde{v}}I\right] \tag{9}$$

In equation (5) and (9), μ represents molecular viscosity modeled by the Sutherland equation as

$$\mu = \mu_{ref}\left(\frac{\tilde{T}}{T_{ref}}\right)^{\frac{3}{2}}\frac{T_{ref} + T_0}{\tilde{T} + T_0} \tag{10}$$

$$\begin{Bmatrix} & \mu_{ref}[\frac{Kg}{ms}] & T_{ref}[K] & T_0[K] \\ Air & 1.716 \times 10^{-5} & 273.15 & 110.4 \\ H_2 & 8.411 \times 10^{-6} & 273.15 & 96.67 \end{Bmatrix}$$

Compressible extension of the Smagorinsky subgrid scale model for the eddy viscosity and heat flux is based on wall-adapting local eddy-viscosity model (WALE) for the eddy-viscosity term [18].

$$\vec{\tau} = \mu_{SGS}\left[\left(\vec{\nabla}.\vec{\tilde{v}} + \vec{\nabla}.\vec{\tilde{v}}^{T}\right) - \frac{2}{3}\vec{\nabla}.\vec{\tilde{v}}I\right] \tag{11}$$

$$\vec{Q} = \mu_{SGS}\frac{C_p}{\mathrm{Pr}_t}\vec{\nabla}\bar{T} \tag{12}$$

$$\mu_{SGS} = \bar{\rho}C_w\Delta_s^2\left|\tilde{S}\right| \tag{13}$$

$$\Delta_s = (\forall_\omega)^{\frac{1}{3}} \tag{14}$$

$$\tilde{S} = \sqrt{\frac{\left(\tilde{S}_{ij}\tilde{S}_{ij}\right)^3}{\left(\bar{S}_{ij}\bar{S}_{ij}\right)^5 + \left(\tilde{S}_{ij}\tilde{S}_{ij}\right)^{\frac{5}{2}}}} \tag{15}$$

$$\tilde{S}_{ij} = \frac{\partial\tilde{u}_i}{\partial x_j} + \frac{\partial\tilde{u}_j}{\partial x_i} \tag{16}$$

Note that in this simulation the thermodynamic properties will not be changed and are homogenously distributed in the domain. No heat transfer to the ambient and no phase change is considered. Molecular viscosity is modeled by the Sutherland equation. Previously it was showed that the Abel-Noble equation of states for real gas modeling with one coefficient (8) is appropriate for high pressure hydrogen release simulation [1], [2], therefore it is employed here.
While there are two species, air and hydrogen, a transport equation is solved separately to determine the concentration of species.

$$\frac{\partial C}{\partial t} + \vec{\nabla}.\left(C\vec{\tilde{v}}\right) = \vec{\nabla}.\vec{\tilde{J}} \quad , \quad \vec{\tilde{J}} = D_f\,\vec{\nabla}C \tag{17}$$

Concentration is zero for pure hydrogen and one for air. The diffusion coefficient for hydrogen in air (D_f) is 6.1×10^{-5} m^2/s at normal temperature and pressure conditions [15]. A linear averaging with respect to concentration is applied for all coefficients.

Although the ratio of specific heats ($\gamma_g = C_p/C_v$) is the same for hydrogen and air, R and the coefficients of Sutherland equation are different. In this case a simple linear averaging with respect to concentration is applied.

$$R = CR_{air} + (1 - C)R_{H_2} \quad (18)$$

$$\mu_{ref} = C\mu_{ref}{}_{air} + (1 - C)\mu_{ref}{}_{H_2} \quad (19)$$

$$T_0 = CT_{0_{air}} + (1 - C)T_{0_{H_2}} \quad (20)$$

The numerical method used here is a mixed finite volume – finite element method. For the temporal term, a second order implicit scheme is applied. Convective fluxes are discretized with the 2nd order Roe-MUSCL (βγ scheme) while a 2nd order finite element method is used for diffusive fluxes. To control undesired oscillations in discontinuities the Van Leer-Van Albada limiter is applied. Since Roe-MUSCL method brings significant dissipation to the numerical solution, which is overwhelming the LES contribution, a self-adaptive coefficient is defined for the upwinding term to reduce its contribution while keeping the method stable. To adjust this coefficient, a dynamic wiggle detection scheme is used [15,17]. Note that to guarantee the stability of the simulation, regions with shocks, high gradient in the Mach number, require full upwind method (γ = 1). During the simulation, the CFL is increased with iterations. The initial and maximum CFL numbers are set as 0.1 and 60, respectively.
In this study, the boundary conditions employed are: adiabatic no-slip / slip wall and non-reflecting pressure outlet as shown in Fig. 1.

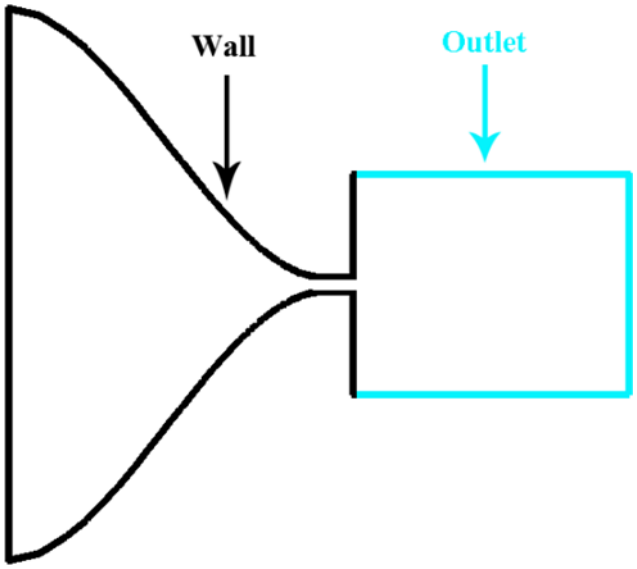

Figure 1. Boundary condition of the computational domain

2.1 Mesh

The computational domain which is illustrated in Fig. 2 contains two zones: a high pressure hydrogen reservoir and a low pressure atmosphere, which are connected with a small cylindrical orifice defined by a diameter D=1 mm and a length L=2 mm. The throat of the nozzle starts at a/L=0, and the exit is at a/L=1 (Fig. 3) and the area is constant. The initial contact surface between hydrogen and air is placed in the middle of the nozzle (a/L = 0.5). An unstructured tetrahedron grid having about 14.8 million grid points is generated and used for all simulations. The grid is densely clustered near the interior wall to capture the boundary layer. For all simulations the y+ is kept around 25 by having the first row mesh size of 2 micrometer and 0.38 micrometer for 10 MPa and 70 MPa, respectively. To obtain the appropriate mesh size of the first element, the mesh is stretched accordingly.

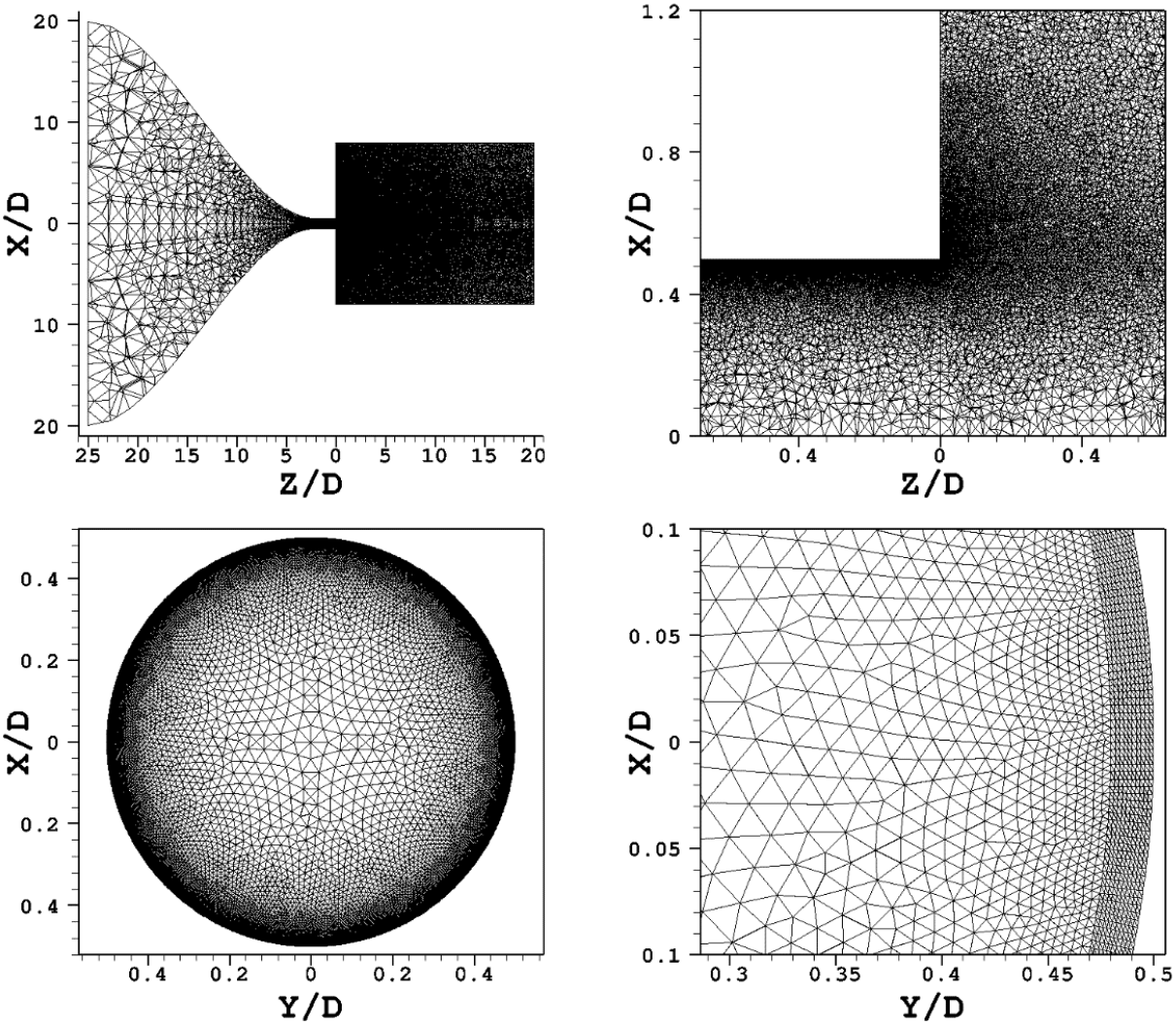

Figure 2. Mesh in the computational domain and at the end of the nozzle exit

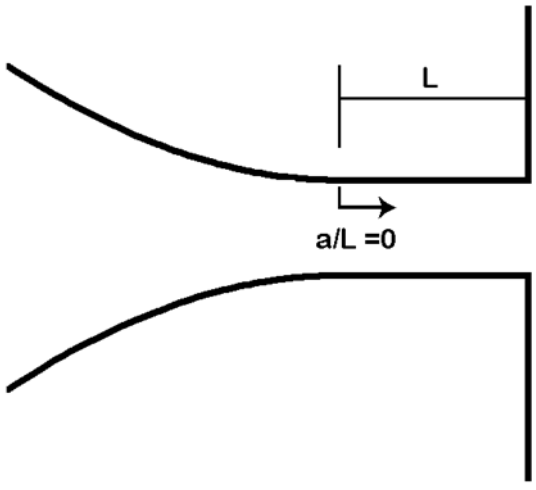

Figure 3. Coordinate system of the nozzle

3.0 RESULTS

The transient simulation starts with the following initial conditions: ambient condition for air (101325 Pa, 300K) and stagnation conditions for hydrogen (10 MPa or 70 MPa, 300 K).

3.1 Analysis of flow field

As indicated earlier, the boundary layer creates a converging-diverging effect that accelerates the flow above Mach number 1.0. To illustrate this effect, the distribution of Mach number inside the release area is shown in Fig. 4 for tank pressures of 10 MPa and 70 MPa after 15 microseconds of release. Note that the boundary layer increases gradually until it start decreases near the exit. It is seen that the Mach number exceeds unity close to the entrance of the nozzle and exist the nozzle at Mach number of 1.28 in both cases. The radial distribution of Mach number is also reported in Fig. 4. Notice that the 70 MPa flow is developing faster but become equal to the 10 MPa at the exit. It is also clear that the boundary layer on the nozzle wall can reach 50% of the radius.

For comparison, the inviscid solutions are also presented after 15 micro-seconds in Fig. 5. Note that in this case there is no boundary layer and the Mach number increases as expected to a value of 1.0 .

To illustrate the effect of the boundary layer on the flow once it exits the nozzle, we analyse the difference between the sonic flow obtained with an inviscid simulation (Euler) and the viscous flow obtained with the LES simulation. In Fig. 6 the centerline values of Mach number, density, temperature and pressure are shown for both cases after 15 microseconds of release. All the quantities are normalized with air initial condition and diameter of orifice. Clearly the inviscid flow is developing outside the reservoir faster than the viscous flow. Studying the position of the lead shock, it can be seen that the inviscid assumption causes faster propagation of the flow and a bigger dispersion cloud. It is clear that the flow is choked by an effective throat area which is smaller than the nozzle area. This leads to a reduction in the flow rate and indicates that the inviscid flow is more conservative while studying auto-ignition because it gives a higher temperature peak. Table 1 provides the mass flow rate values calculated for both inviscid and viscous simulation at 15 micro-seconds after release. The difference is significant and requires further investigation to validate these numbers.

Table 1. Mass flow rates at 15 micro-seconds.

LES 10MPa	Euler 10MPa	LES 70MPa	Euler 70MPa
0.003263 kg/s	0.004546 kg/s	0.018814 kg/s	0.029415 kg/s

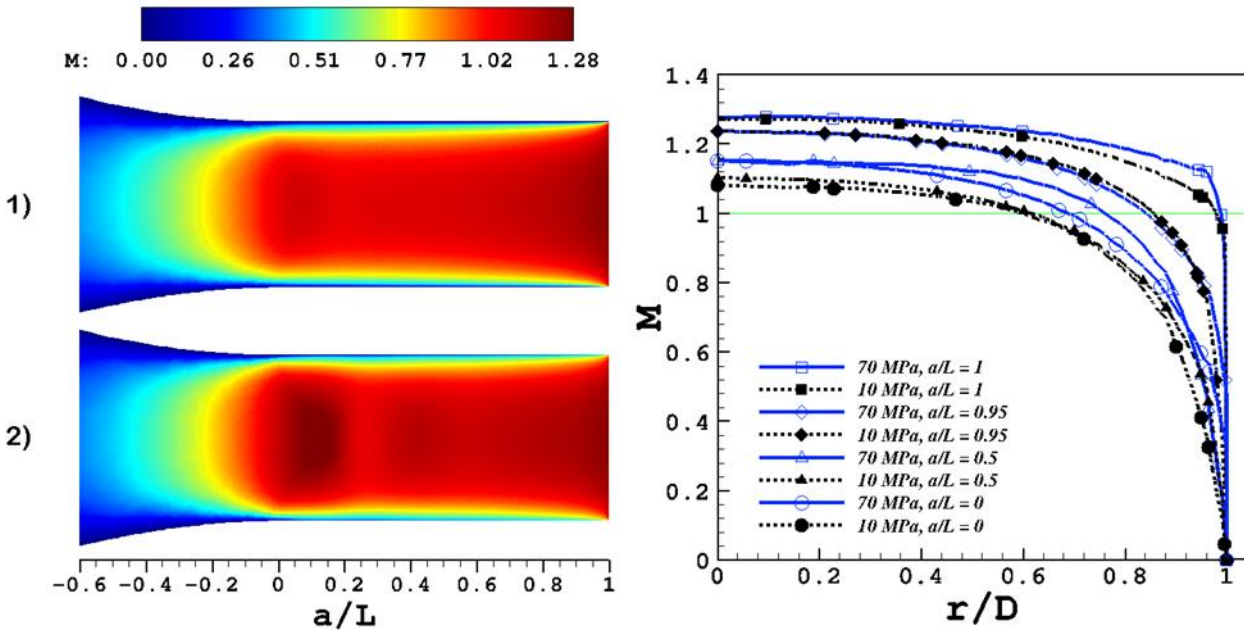

Figure 4. Viscous Mach number distribution inside the release pipe after 15 micro-second of release for 1) 10 MPa and 2)70 MPa of tank pressure change to iso-lines with one line at Mach 1

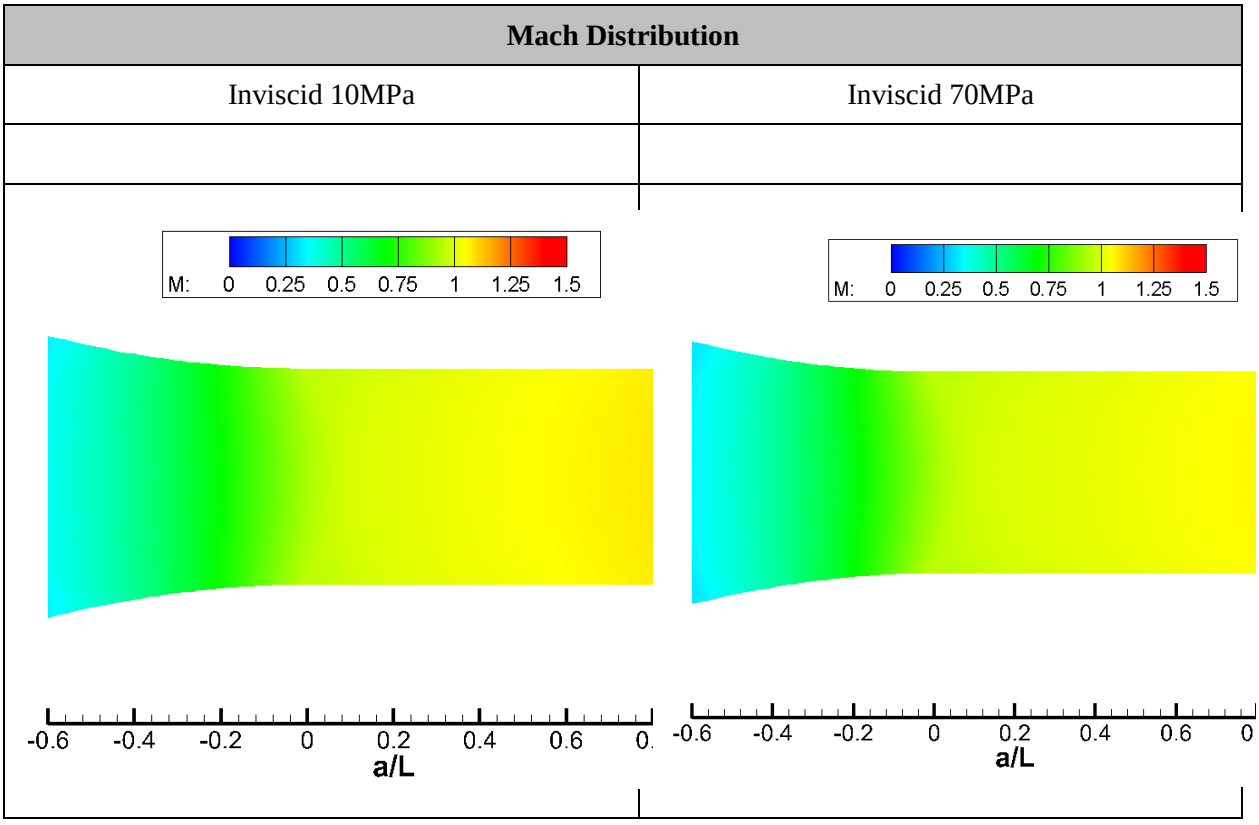

Figure 5. Inviscid Mach number distribution inside the release pipe after 15 micro0second of release for left) 10 MPa and right) 70 MPa of tank pressure

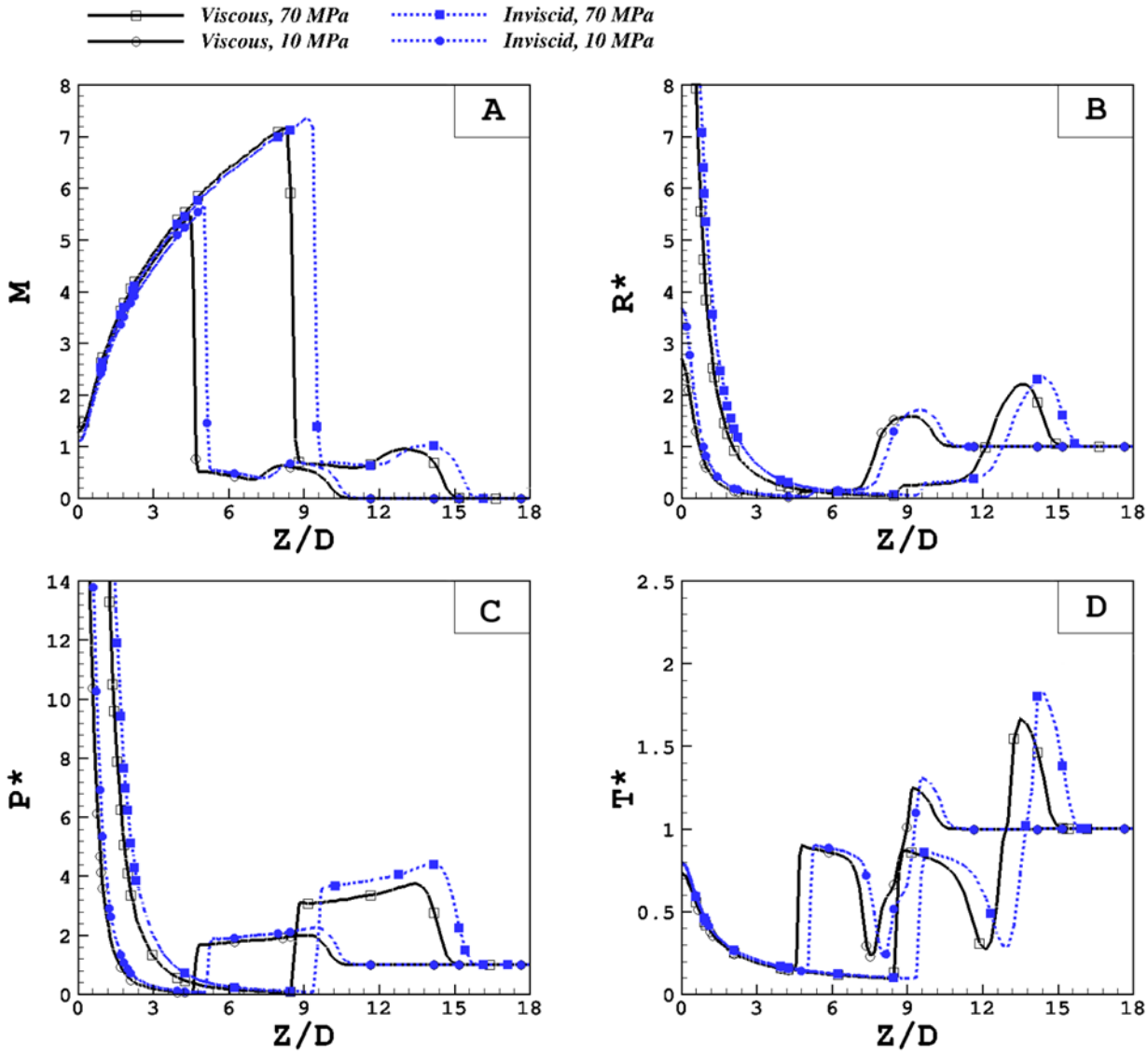

Figure 6. Centerline values of hydrogen jet release from 1mm orifice after 15 microsecond of release for A) Mach number, B) density, C) pressure, and D) temperature

4.0 CONCLUSION

A model based on Large Eddy Simulation is presented to capture the viscous boundary layer developing inside the exit constant area nozzle when hydrogen is released from a high pressure reservoir (up to 70 MPa). To have accurate results, a fine mesh near the wall of the exit duct is employed with a grid having 14.8 million nodes. The simulation shows that the viscous boundary layer causes a convergent divergent throat effect which leads to a supersonic flow in the nozzle. This effect also shocks the flow and the mass flow rate is reduced compared to a sonic flow. Therefore, the peak temperature on the center line is higher for Euler simulations compare to viscous simulations. We conclude that inviscid (Euler) simulations are less accurate but more conservative for safety studies because they predict higher mass flow and higher temperatures.

REFERNCES

1. Mohamed, K. and Paraschivoiu, M., Real gas simulation of hydrogen release from a high-pressure chamber, *International Journal of Hydrogen Energy*, **30**, no. 8, 2005, pp. 903-912.
2. Khaksarfard, R., Kameshki, M. R., and Paraschivoiu, M., Numerical simulation of high pressure release and dispersion of hydrogen into air with real gas model, *Shock Waves*, **20**, no. 3, 2010, pp. 205-216.
3. Chernyavsky, B., Wu, T.C., Peneau, F., Benard, P., Oshkai, P. and Djilali, N., Numerical and experimental investigation of buoyant gas release: Application to hydrogen jets, *International Journal of Hydrogen Energy*, **36**, 2011, pp. 2645-2655.
4. Radulescu, M. I. and Law, C. K. , The transient start of supersonic jets, *J. Fluid Mech.*, **578**, 2007, pp. 331–369.
5. Papanikolaou, E., Baraldi, D., Kuznetsov, M., and Venetsanos, A., Evaluation of notional nozzle approaches for CFD simulations of free-shear under-expanded hydrogen jets, *International Journal of Hydrogen Energy*, **37**, no. 23, 2012, pp. 18563-18574.
6. Lijo, V., Kim, H. D. , Setoguchi, T. and Matsuo, S., Study on the compressible viscous flows through a straight pipe, *J. Mech. Sci. Technol.*, **25**, no. 2, 2011, pp. 341–347.
7. Kubo, K., Miyazato, Y., and Matsuo, K., Study of choked flows through a convergent Nozzle, *Journal of Thermal Science*, **19**, no. 3, 2010, pp. 193-197.
8. Ding, H., Wang, C. and Zhao, Y., Flow characteristics of hydrogen gas through a critical nozzle, Int. *J. Hydrogen Energy*, **39**, no. 8, 2014, pp. 3947–3955.
9. Nagao, J., Matsuo, S., Mohammad, M., Setoguchi, T. and Kim H.D., Numerical study on characteristics of real gas flow through a critical nozzle, *Int. J. Turbo Jet Engines*, **29**, no. **1**, 2012, pp. 21–27.
10. Von Lavante, E., Zachcial, A. ,Nath, B.,and Dietrich, H., Numerical and experimental investigation of unsteady effects in critical Venturi nozzles, *Flow Meas. Instrum.*, **11**, no. 4, 2000, pp. 257–264.
11. Velikorodny, Alexey; Kudriakov, Sergey, Numerical study of the near-field of highly under-expanded turbulent gas jets, *Int. J. Hydrogen Energy*, **37**, no. 22, 2012, pp. 17390-17399.
12. Kim, J.-H., Kim, H.-D. , Setoguchi, T. and Matsuo S., A computational study of real gas flows through a critical nozzle," *Proc. Inst. Mech. Eng. Part C J. Mech. Eng. Sci.*, **223**, no. 3, 2009., pp. 617–626.
13. Morioka, T., Nakao, S-I., Ishibashi, M., Characteristics of Critical Nozzle Flow Meter for Measuring High-Pressure Hydrogen Gas, *Transactions of the Japan Society of Mechanical Engineers Series B*, **77**, no. 776, 2011, pp. 1088-1097.
14. Shishehgaran, N. and Paraschivoiu, M., CFD based simulation of hydrogen release through elliptical orifices, *International Journal of Hydrogen Energy*, **39**, no. 35, 2014, pp. 20350-20356.
15. Markert, F., Melideo D. and Baraldi, D., Numerical analysis of accidental hydrogen releases from high pressure storage at low temperatures, *International Journal of Hydrogen Energy*, **39**, no. 14, 2014, pp. 7356-7364.
16. Tajallipour N., Large eddy simulations for compressible turbulent jet flows, PhD thesis, Concordia University, 2009.
17. Péneau, F.,Pedro, G., Oshkai, O., Bénard, P., and Djilali, N., Transient supersonic release of hydrogen from a high pressure vessel: A computational analysis, *International Journal of Hydrogen Energy*, **34**, 2009, pp. 5817-5827.
18. Ducros, F., Nicoud, F., and Poinsot, T., Wall-adapting local eddy-viscosity models for simulations in complex geometries." International Conference on Computational Conference. 1998.
19. Tajallipour, N., Babaee Owlam, B., and Paraschivoiu, M., Self-Adaptive Upwinding for Large Eddy Simulation of Turbulent Flows on Unstructured Elements, *AIAA J. Aircr.*, **46**, no. 3, 2009, pp. 915–926.